RANS model development at LLNL for the prediction of turbulent mixing

UM/NASA Symposium on Advances in Turbulence Modeling

Brandon Morgan

11 July 2017

LLNL-PRES-733799

This work was performed under the auspices of the U.S. Department of Energy by Lawrence Livermore National Laboratory under contract DE-AC52-07NA27344. Lawrence Livermore National Security, LLC

Lawrence Livermore National Laboratory

ICF target performance is sensitive to effects of turbulent mixing, driving RANS development

- In inertial confinement fusion (ICF) applications at the National Ignition Facility (NIF), laser energy is converted to x-rays in order to implode a spherical deuterium-tritium (DT) capsule and achieve thermonuclear energy release.
- This process is sensitive to turbulent mixing of ablator material into the DT hot spot.
- Mixing is driven by Rayleigh-Taylor (RT) and Richtmyer-Meshkov (RM) instabilty growth

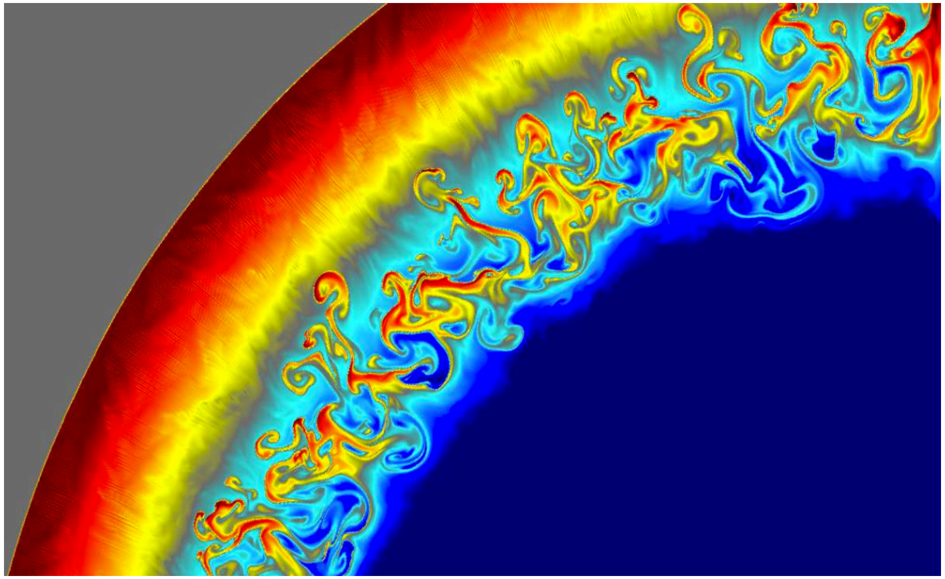

Duffell, P.C. *App J.* (2016)

For mixing applications, the buoyancy production term is generally dominant

- Consider the transport of turbulence kinetic energy, *k*:

$$\bar{\rho}\frac{\partial k}{\partial t} + \bar{\rho}\tilde{u}_j\frac{\partial k}{\partial x_j} = \underbrace{R_{ij}\frac{\partial \tilde{u}_i}{\partial x_j}}_{\text{production}} - \underbrace{\overline{t_{ji}\frac{\partial u_i''}{\partial x_j}}}_{\text{dissipation}} + \underbrace{\frac{\partial}{\partial x_j}\left[\overline{t_{ji}u_i''} - \frac{1}{2}\overline{\rho u_j'' u_i'' u_i''} - \overline{p' u_j''}\right]}_{\text{turbulent transport}} - \underbrace{\overline{u_i''}\frac{\partial \bar{p}}{\partial x_i}}_{\text{buoyancy}} + \underbrace{\overline{p'\frac{\partial u_i''}{\partial x_i}}}_{\text{p. dilatation}}$$

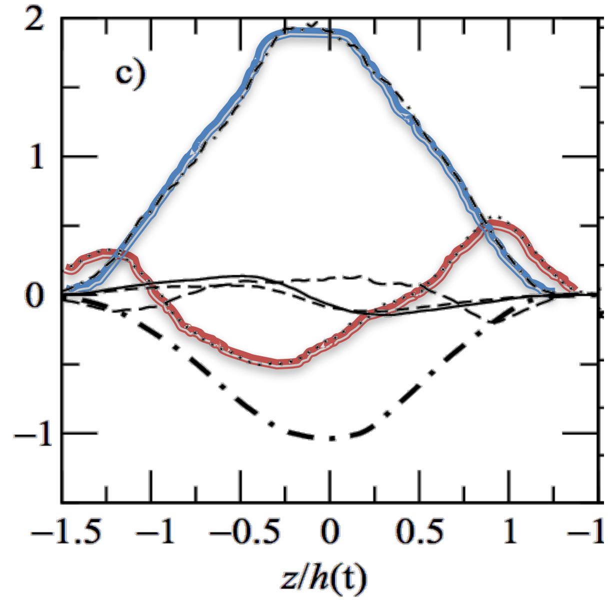

TKE budget across an RT mixing layer (At = 0.5). Livescu, et al. *J. Turb.* 2009

Closure of the mass-flux velocity is key for for turbulent mixing applications

- Consider a model transport equation for *k*:
  - We now introduce the turbulent length scale, $\mathrm{L} = k^{3/2}/\epsilon$, and the mass-flux velocity, $a_j = -\widetilde{u_j''}$

$$\bar{\rho}\frac{Dk}{Dt} = \underbrace{\bar{\rho}\tau_{ij}\frac{\partial \tilde{u}_i}{\partial x_j}}_{\text{production}} \underbrace{- C_D\frac{\bar{\rho}\,(2k)^{3/2}}{L}}_{\text{dissipation}} + \underbrace{\frac{\partial}{\partial x_i}\left(\frac{\mu_t}{N_k}\frac{\partial k}{\partial x_i}\right)}_{\text{turbulent transport}} + \underbrace{a_j\frac{\partial \bar{p}}{\partial x_i}}_{\text{buoyancy}}$$

- Closure of the mass-flux velocity leads to a family of two- and three-equation Boussinesq models favored at LLNL.
  - An algebraic gradient diffusion closure leads to the KL model (Dimonte & Tipton, *Phys. Fluids* 2006)
  - Solving a transport equation for a_i leads to the KLA model (Banerjee, et al., *Phys. Rev. E* 2010; Morgan & Wickett, *Phys. Rev. E* 2015).

Similarity analysis is used to derive constraints on model constants

- Assuming an ansatz of a self-similar growth allows us to derive a set of constraints on model constants parameterized by experimentally observable quantities (Morgan & Wickett, PRE, 2015):

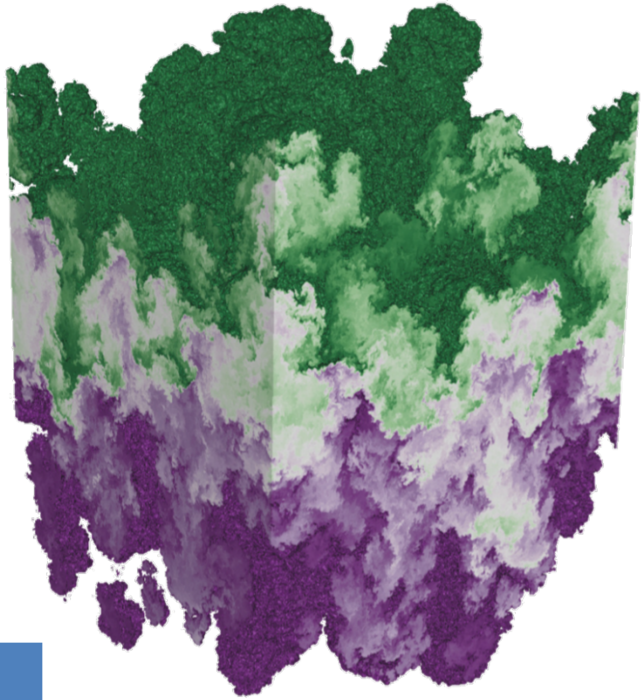

Constant	Description	Typical Value
α_b	RT bubble growth rate	0.060
θ	RM growth rate	0.25
$E_k/\Delta PE$	RT energy ratio	0.50
n	HIT decay constant	-1.11

These constraints enforce a particular profile and growth rate

- Adhering to these constraints enforces a quadratic TKE profile for a 1D Rayleigh-Taylor mixing layer (At = 0.05)…

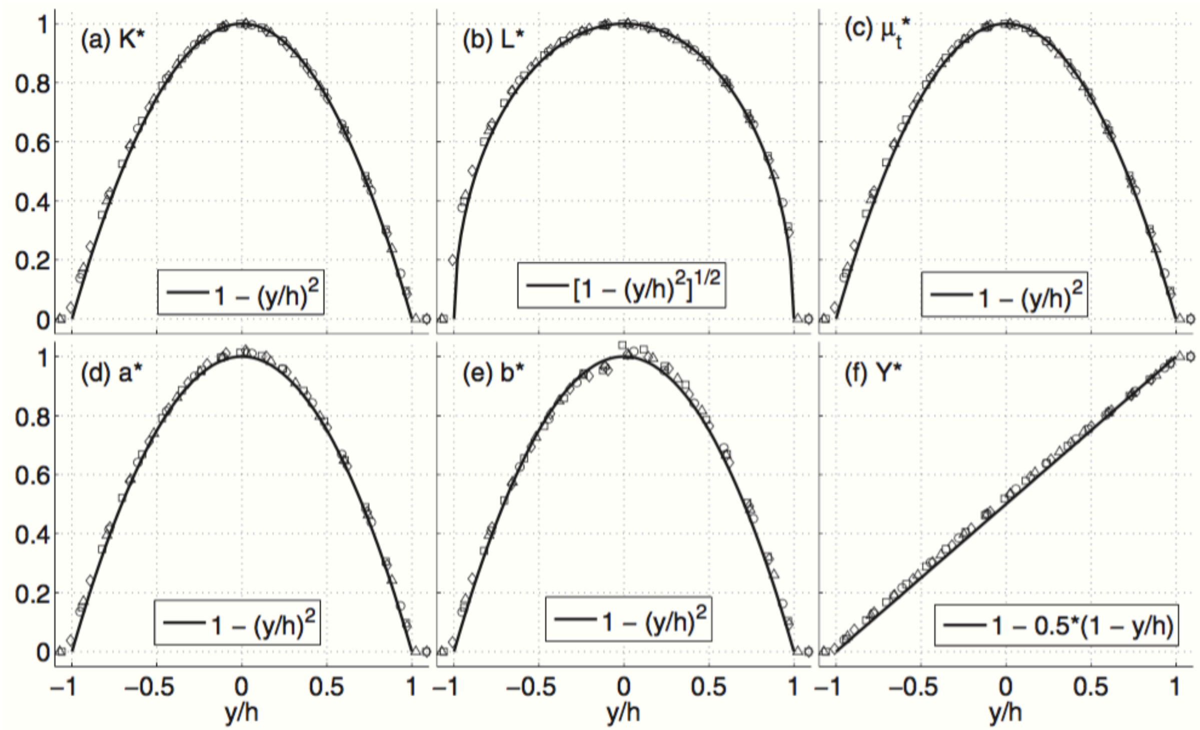

FIG. 1. Normalized profiles obtained for a one-dimensional RT mixing layer of $A_T = 0.05$ at non-dimensional time $\tau = t(A_T g/\lambda_0)^{1/2} =$ 324 (□), 648 (○), 972 (△), and 1296 (◇): (a) $K^* = k/K_0$, (b) $L^* = L/L_0$, (c) $\mu_t^* = \mu_t/(C_\mu \rho L_0 \sqrt{2K_0})$, (d) $a^* = (A_T^2 - 1)a_y/(C_B A_T \sqrt{2K_0})$, (e) $b^* = (1 - A_T^2)b/A_T^2$, and (f) $Y^* \equiv$ heavy fluid mass fraction.

These constraints enforce a particular profile and growth rate

- … and the expected growth rate is recovered

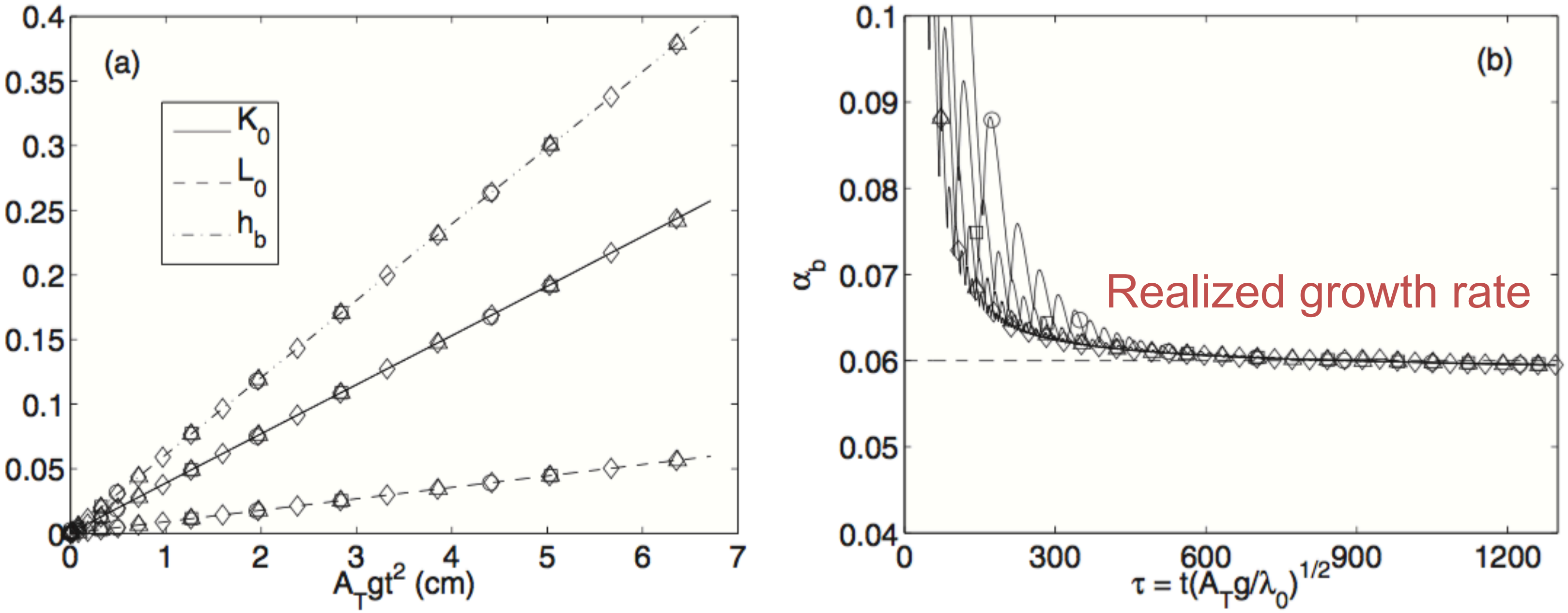

FIG. 2. Convergence of a one-dimensional RT mixing layer at $A_T = 0.05$ with grid resolution of 200 (◯), 400 (□), 800 (△), and 1600 (◊) zones. (a) Solutions of h_b, K_0, and L_0. Dimensions are in cm for h_b and L_0 and 10^{-9} $(\mathrm{cm}/\mu\mathrm{s})^2$ for K_0. (b) Time history of $\alpha_b = h_b/A_T gt^2$.

These constraints enforce a particular profile and growth rate

- A quadratic TKE profile yields reasonable agreement in comparisons with LES ...

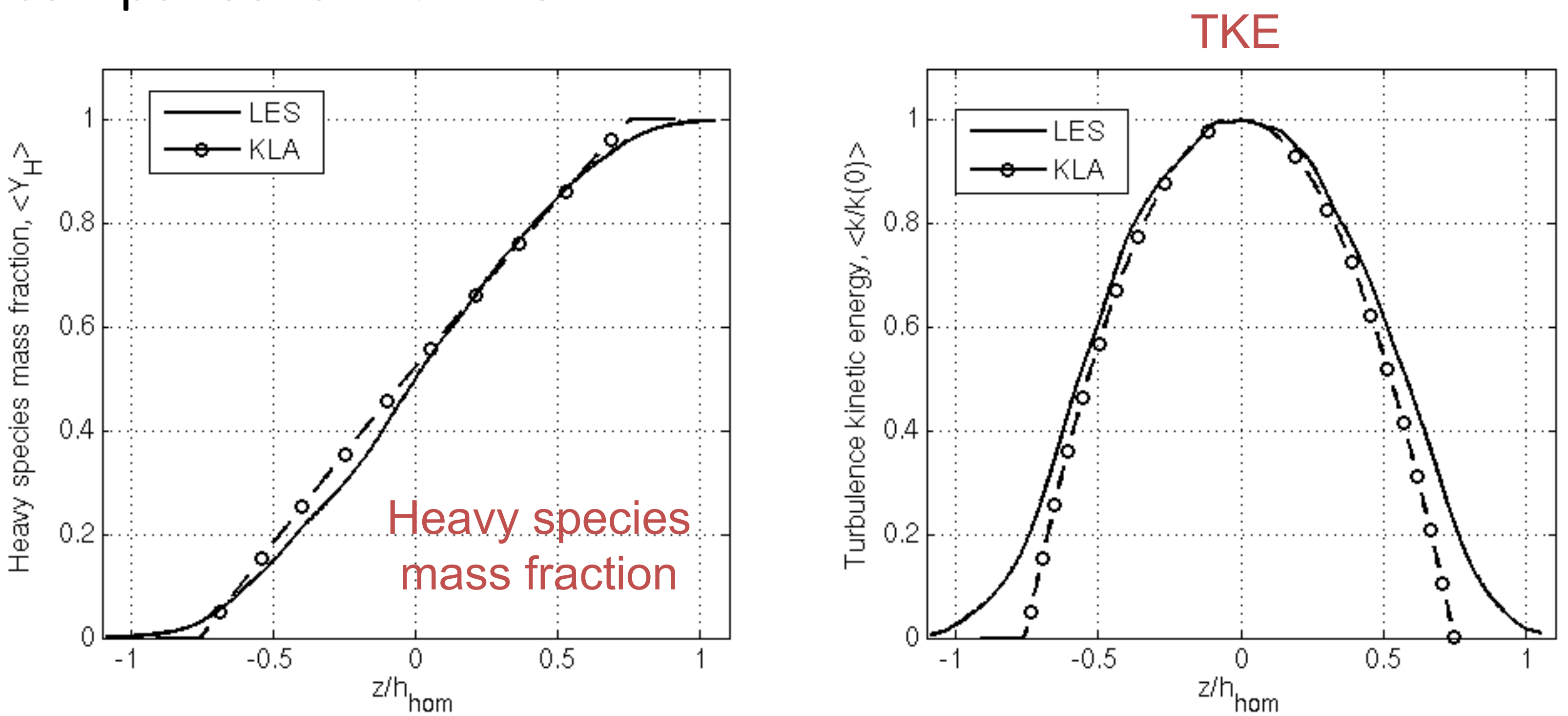

Heavy species mass fraction (left) and normalized TKE profiles (right) for LES and RANS of an RT mixing layer at At = 0.05. Morgan et al., *J. Turbul.* 2017. DOI 10.1080/14685248.2017.1343477

These constraints enforce a particular profile and growth rate

- ... and in comparisons with experiment for Richtmyer-Meshkov mixing layer growth

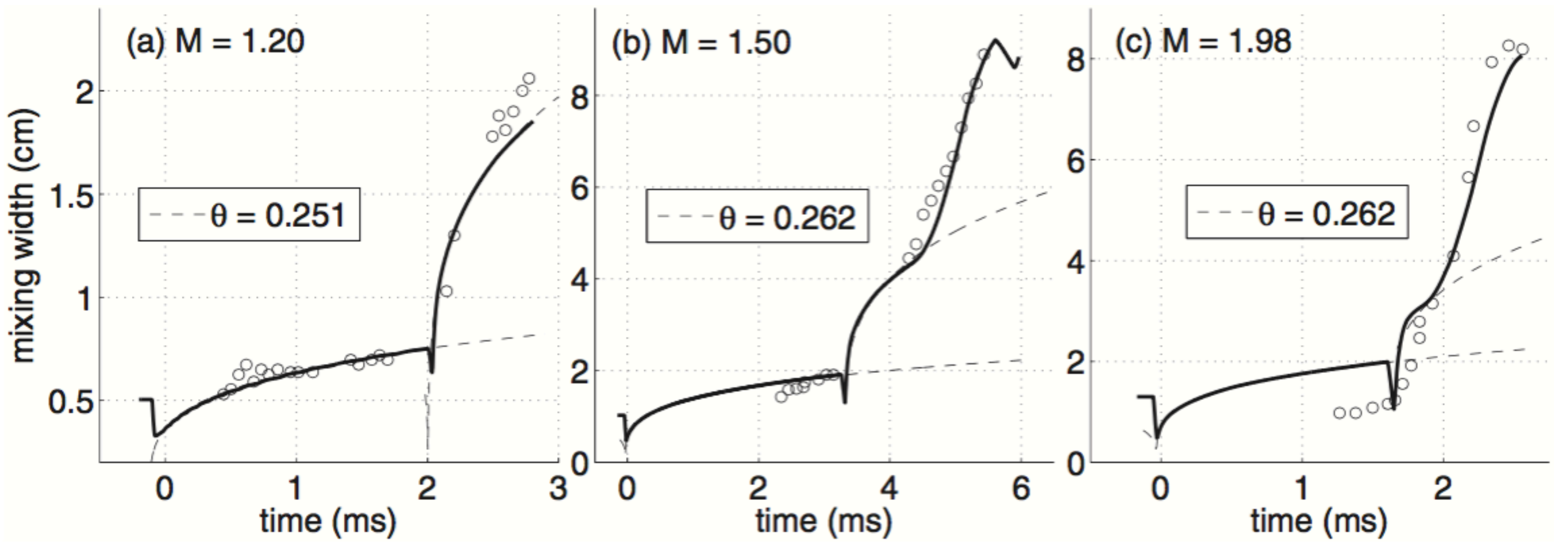

FIG. 4. Mixing width profiles calculated for three different shock tube experiments: (*a*) Leinov *et al.* experiment 1570 [18] ($h_0 = 0.110$ cm, test section = 23.5 cm), (b) Vetter and Sturtevant experiment 85 [19] ($h_0 = 0.224$ cm, test section = 60.0 cm), and (c) Vetter and Sturtevant experiment 87 [19] ($h_0 = 0.283$ cm, test section = 49.0 cm). Symbols (◯) indicate experimental data. Dashed lines are power law profiles fit to the simulation data.

This is a good starting point, but reality is never so ideal. What about transition?

- Mixing layers do not start out in a self-similar regime. It may take several bubble merger generations to achieve such a state

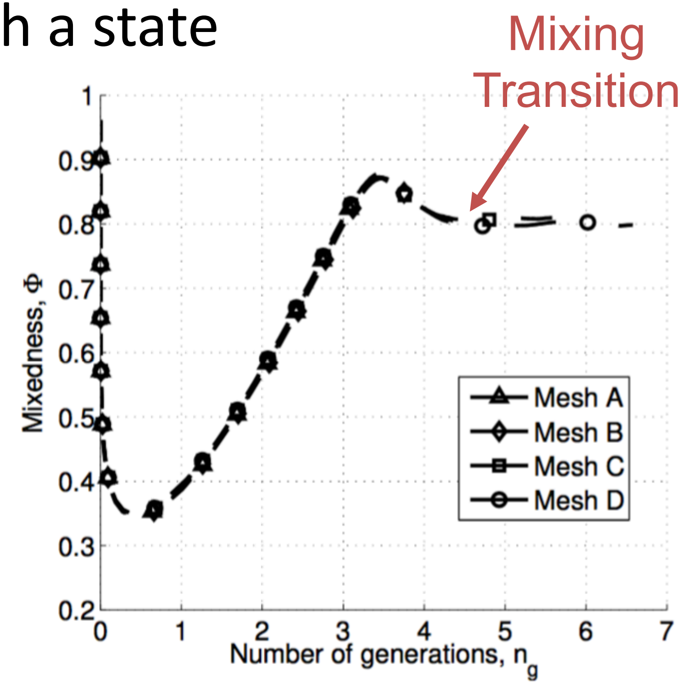

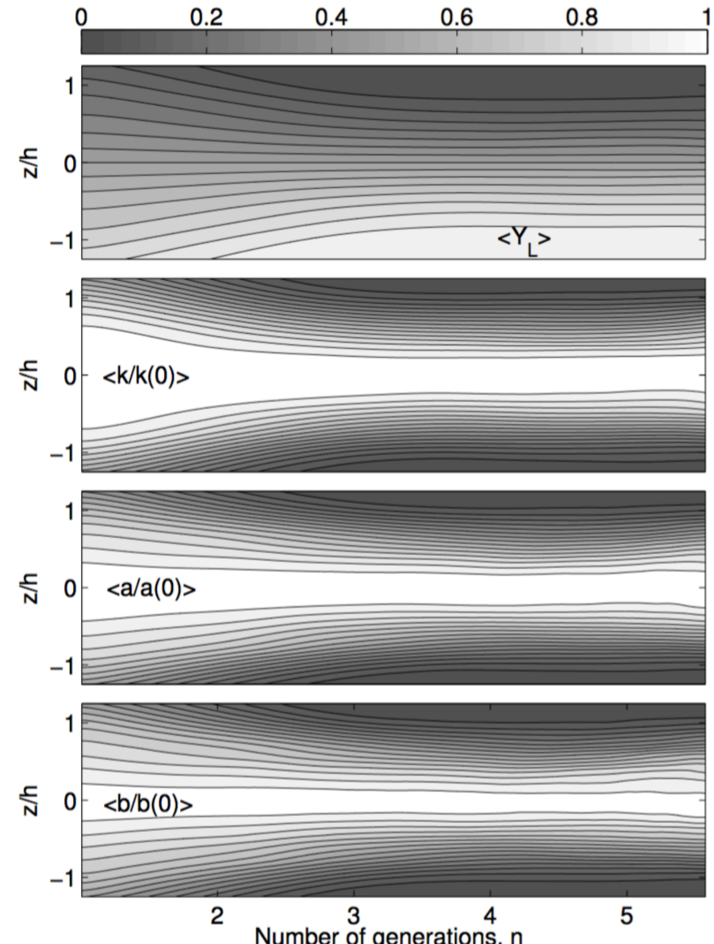

Mixedness vs. generation (left) and normalized contours (right) for LES of an RT mixing layer at At = 0.05. Morgan et al., *J. Turbul.* 2017. DOI 10.1080/14685248.2017.1343477

By design, the RANS model does not capture transition to turbulence.

- Transition to self-similarity is therefore also different from LES.

$$\sigma_f\left(n_g\right) \equiv 1 - \int_{-\infty}^{\infty} \frac{\left|\frac{\partial\langle f\rangle}{\partial n_g}\right|}{\sqrt{\left(\frac{\partial\langle f\rangle}{\partial n_g}\right)^2 + \left(\frac{\partial\langle f\rangle}{\partial \chi}\right)^2}} \mathrm{d}\chi \,.$$

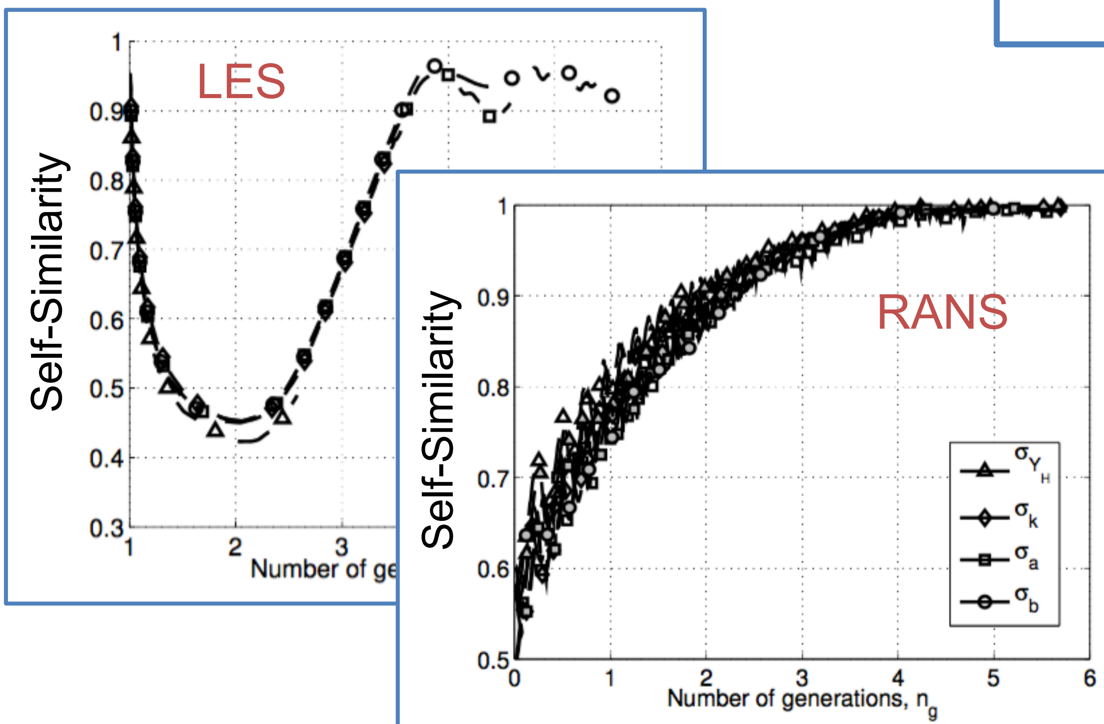

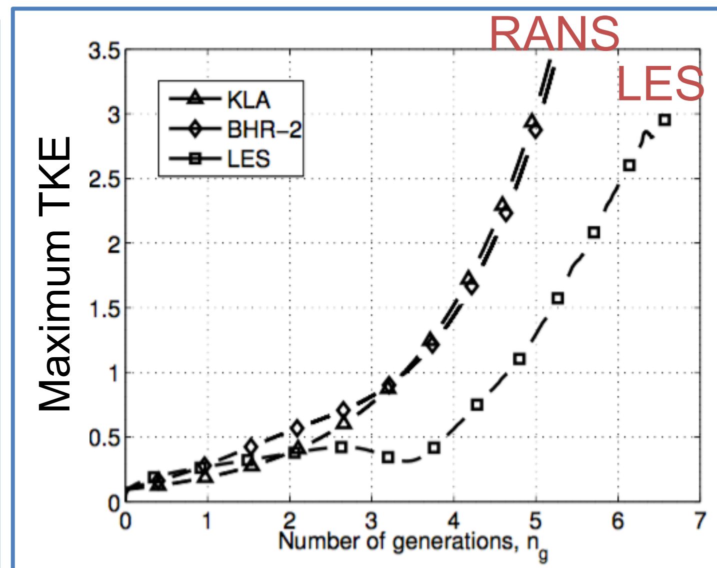

Self-similarity parameter (left) and TKE evolution (right) for LES and RANS of an RT mixing layer at At = 0.05. Morgan et al., *J. Turbul.* 2017. DOI 10.1080/14685248.2017.1343477

Experiment designers are additionally applying these models to problems in two dimensions.

- **Reality is not 1D**. NIF capsules, for instance, may include two- or three-dimensional features
- Can a RANS model designed to reproduce one-dimensional mixing layer growth rates be successfully applied in multidimensional simulations?

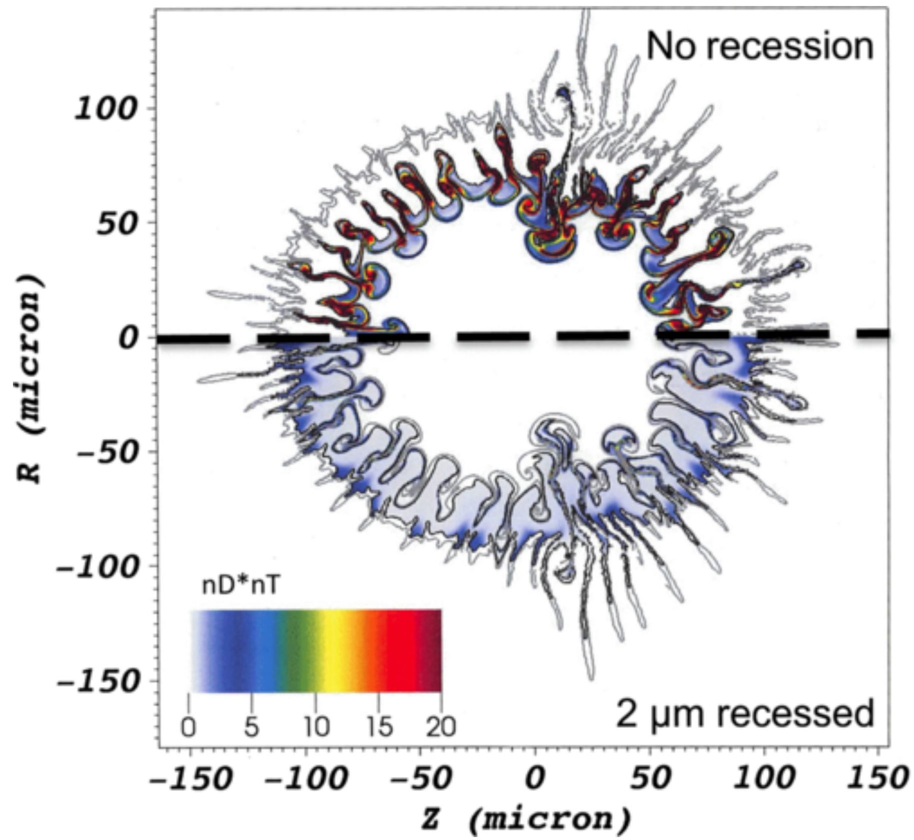

The product of D and T number densities, for simulations with 0µm and 2µm recessed CD layer, showing the spatial distribution of shell-gas mix. Smalyuk et al. *Phys. Rev. Lett.* **112**, 025002 (2014).

As engineers push RANS beyond an idealized design space, can our models keep up?

- Model development at LLNL is driven primarily by the need to accurately predict RT and RM instability growth
- Our models do a good job at predicting idealized growth under the assumption of a 1D, fully developed mixing layer
- Experiment designers apply these models in regimes in which model assumptions may break down
  - Transitional turbulence
  - Two-dimensional simulations
  - Combined instabilities (e.g. RT + KH)

Can data-driven approaches help correct errors when a model is pushed to the limits of its design assumptions?

Backup Slides

Backup Slides: The KL model

$$\frac{D\overline{\rho}}{Dt} = -\overline{\rho}\frac{\partial \widetilde{u}_i}{\partial x_i} \tag{1}$$

$$\overline{\rho}\frac{D\widetilde{Y}_\alpha}{Dt} = \frac{\partial}{\partial x_i}\left(\frac{\mu_t}{\mathrm{Sc}_T}\frac{\partial \widetilde{Y}_\alpha}{\partial x_i}\right) \tag{2}$$

$$\overline{\rho}\frac{D\widetilde{u}_j}{Dt} = -\frac{\partial}{\partial x_j}\left(\overline{p} + p_t\right) + \nu_s\frac{\partial \tau_{ij}}{\partial x_i} + \overline{\rho} g_j \tag{3}$$

$$\overline{\rho}\frac{D\widetilde{e}}{Dt} = -\overline{p}\frac{\partial \widetilde{u}_i}{\partial x_i} + b_t\frac{\mu_t}{\overline{\rho}^2}\left(\frac{\partial \overline{\rho}}{x_i}\frac{\partial \overline{p}}{x_i}\right) + d_t\frac{\overline{\rho}k^{3/2}}{L} + \frac{\partial}{\partial x_j}\left(\frac{\mu_t}{\mathrm{Pr}_T}\frac{\partial \widetilde{e}}{\partial x_j}\right) \tag{4}$$

$$\overline{\rho}\frac{Dk}{Dt} = \nu_s\tau_{ij}\frac{\partial \widetilde{u}_i}{\partial x_j} - p_t\frac{\partial \widetilde{u}_i}{\partial x_i} - b_t\frac{\mu_t}{\overline{\rho}^2}\left(\frac{\partial \overline{\rho}}{x_i}\frac{\partial \overline{p}}{x_i}\right) - d_t\frac{\overline{\rho}k^{3/2}}{L} + \frac{\partial}{\partial x_i}\left(\frac{\mu_t}{k_{num}}\frac{\partial k}{\partial x_i}\right) \tag{5}$$

$$\overline{\rho}\frac{DL}{Dt} = l_{1t}\overline{\rho}L\frac{\partial \widetilde{u}_i}{\partial x_i} + l_{2t}\overline{\rho}\sqrt{2k} + \frac{\partial}{\partial x_i}\left(\frac{\mu_t}{l_{num}}\frac{\partial L}{\partial x_i}\right) \tag{6}$$

$$p_t = \frac{2}{3}\overline{\rho}k, \quad \mu_t = a_t\overline{\rho}L\sqrt{k}, \quad \tau_{ij} = 2\mu_t S_{ij}, \quad S_{ij} = \frac{1}{2}\left(\frac{\partial \widetilde{u}_i}{\partial x_j} + \frac{\partial \widetilde{u}_j}{\partial x_i}\right) - \frac{1}{3}\frac{\partial \widetilde{u}_k}{\partial x_k}\delta_{ij} \tag{7}$$

Backup Slides: The KLA model

$$\frac{D\overline{\rho}}{Dt} = -\overline{\rho}\frac{\partial \widetilde{u}_i}{\partial x_i} \tag{8}$$

$$\overline{\rho}\frac{D\widetilde{Y}_\alpha}{Dt} = \frac{\partial}{\partial x_i}\left(\frac{\mu_t}{\mathrm{Sc}_T}\frac{\partial \widetilde{Y}_\alpha}{\partial x_i}\right) \tag{9}$$

$$\overline{\rho}\frac{D\widetilde{u}_j}{Dt} = -\frac{\partial}{\partial x_j}\left(\overline{p} + p_t\right) + \nu_s\frac{\partial \tau_{ij}}{\partial x_i} + \overline{\rho}g_j \tag{10}$$

$$\overline{\rho}\frac{D\widetilde{e}}{Dt} = -\overline{p}\frac{\partial \widetilde{u}_i}{\partial x_i} - b_t A_i\frac{\partial \overline{p}}{\partial x_i} + d_t\frac{\overline{\rho}k^{3/2}}{L} + \frac{\partial}{\partial x_j}\left(\frac{\mu_t}{\mathrm{Pr}_T}\frac{\partial \widetilde{e}}{\partial x_j}\right) \tag{11}$$

$$\overline{\rho}\frac{Dk}{Dt} = \nu_s\tau_{ij}\frac{\partial \widetilde{u}_i}{\partial x_j} - p_t\frac{\partial \widetilde{u}_i}{\partial x_i} + b_t A_i\frac{\partial \overline{p}}{\partial x_i} - d_t\frac{\overline{\rho}k^{3/2}}{L} + \frac{\partial}{\partial x_i}\left(\frac{\mu_t}{k_{num}}\frac{\partial k}{\partial x_i}\right) \tag{12}$$

$$\overline{\rho}\frac{DL}{Dt} = l_{1t}\overline{\rho}L\frac{\partial \widetilde{u}_i}{\partial x_i} + l_{2t}\overline{\rho}\sqrt{2k} + \frac{\partial}{\partial x_i}\left(\frac{\mu_t}{l_{num}}\frac{\partial L}{\partial x_i}\right) \tag{13}$$

$$\overline{\rho}\frac{DA_j}{Dt} = B\frac{\partial \overline{p}}{\partial x_j} - a_{1t}\frac{p_t}{\overline{\rho}}\frac{\partial \overline{\rho}}{\partial x_j} - a_{2t}\frac{\tau_{ij}}{\overline{\rho}}\frac{\partial \overline{\rho}}{\partial x_i} - a_{3t}\overline{\rho}A_j\frac{k^{1/2}}{L} + \frac{\partial}{\partial x_i}\left(\frac{\mu_t}{a_{num}}\frac{\partial A_j}{\partial x_i}\right) \tag{14}$$

$$B = \overline{\rho}\left(\frac{\sum_\alpha \frac{v_\alpha}{\rho_\alpha + c\overline{\rho}}}{\sum_\alpha \frac{v_\alpha \rho_\alpha}{\rho_\alpha + c\overline{\rho}}}\right) - 1 \tag{15}$$

$$p_t = \frac{2}{3}\overline{\rho}k, \quad \mu_t = a_t\overline{\rho}L\sqrt{k}, \quad \tau_{ij} = 2\mu_t S_{ij}, \quad S_{ij} = \frac{1}{2}\left(\frac{\partial \tilde{u}_i}{\partial x_j} + \frac{\partial \tilde{u}_j}{\partial x_i}\right) - \frac{1}{3}\frac{\partial \tilde{u}_k}{\partial x_k}\delta_{ij} \tag{16}$$

Backup Slides: The connection between generation number and time

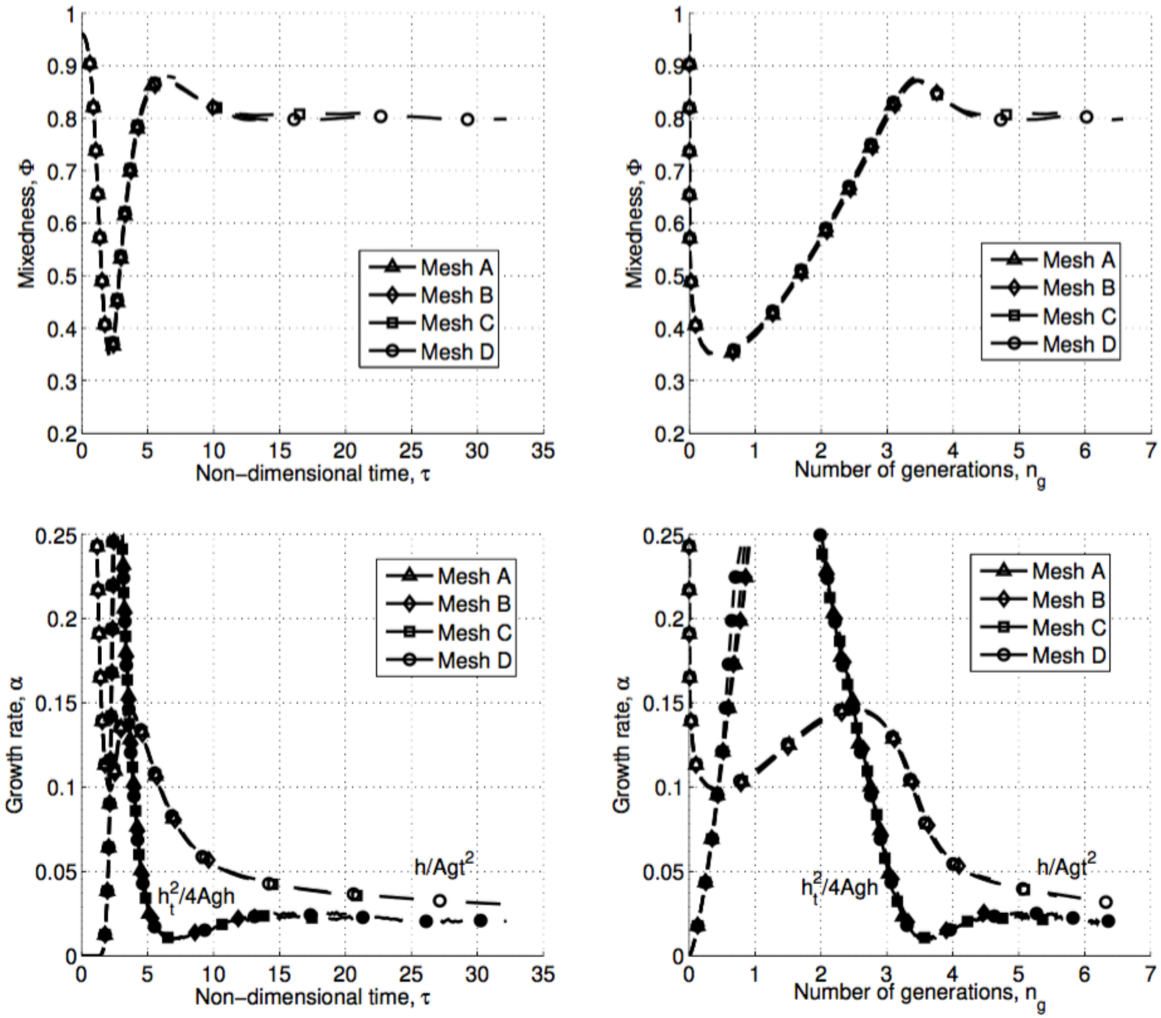

Generation Number

$$n_g\left(t\right) \equiv \log_2\left(\frac{h(t)}{h(0)}\right)$$

Mixedness

$$h \equiv 4\int_{-2\pi}^{2\pi}\overline{Y_H\left(1-Y_H\right)}\mathrm{d}z$$

$$h_{hom} \equiv 4\int_{-2\pi}^{2\pi}\overline{Y_H}\left(1-\overline{Y_H}\right)\mathrm{d}z$$

$$\Phi \equiv \frac{h}{h_{hom}} = 1 - 4\frac{\int_{-2\pi}^{2\pi}\overline{Y_H' Y_H'}\mathrm{d}z}{h_{hom}}$$

Backup Slides: Self-similar evolution of RANS models

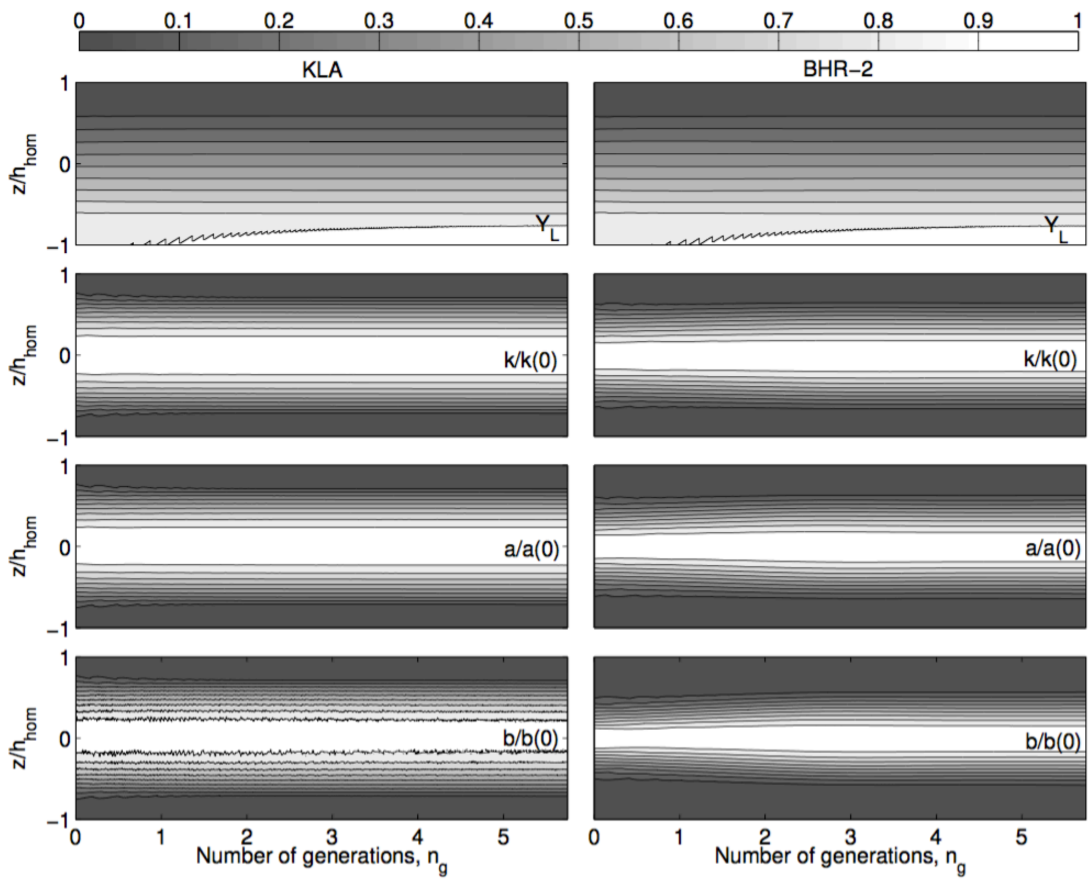

Figure 12. Contours of RANS profiles as a function of time and space. From top to bottom: light species mass fraction $\overline{Y}_L$, turbulence kinetic energy k, mass-flux velocity a, and density-specific-volume correlation b. Results obtained with the k-L-a model are plotted in the left column, and results obtained with the BHR-2 model are plotted in the right column. k, a, and b profiles are normalized by the value at $\chi = 0$.

Lawrence Livermore National Laboratory